Bulletin of the Seismological Society of America, Vol. 83, No. 4, pp. 1167–1183, August 1993

M_L:M_0 AS A REGIONAL SEISMIC DISCRIMINANT

BY BRADLEY B. WOODS, SHARON KEDAR, AND DONALD V. HELMBERGER

ABSTRACT

The m_b:M_S ratio determined by teleseismic observations has proven to be an effective discriminant, for explosive sources tend to be significantly richer in short-period energy than are earthquakes. Unfortunately, this method is limited by the detection threshold of teleseismic surface waves. However, recent advances in instrumentation allowing low amplitude surface wave measurements coupled with new analytical techniques make it feasible to use regional waveform data to determine the long-period source excitation level of low magnitude events. We propose using the ratio of M_L (local magnitude) to M_0 (scalar seismic moment) as an analogous regional discriminant. We applied this criterion to a data set of 299 earthquakes and 178 explosions and found that this ratio seems to be diagnostic of source type. For a given M_0, the M_L of an explosion is more than 0.5 magnitude units larger than that of an earthquake. This separation of populations with respect to source type can be attributed to the fact that M_L is a short-period (1 Hz) energy measurement, whereas seismic moment is determined from long-period body wave phases (period > 4 s) and surface waves (10 to 40 sec). Using regional stations with sources 200 to 600 km away, the effective threshold for magnitude measurements for this discriminant is found to be $M_L = 3.1$ for earthquakes and $M_L = 3.6$ for explosions. This method does require the determination of regional crustal models and path calibrations from master events or by other means.

INTRODUCTION

In this era of increased concern regarding the proliferation of nuclear weapons, the need for effective seismic discrimination techniques is as important as ever. As more countries attain or near the technology threshold needed to develop nuclear weapons, more regions of the world need to be monitored for verification purposes. Effective discrimination methods that can make use of historical seismic data and don't require elaborate, costly large-scale arrays, are of considerable interest.

One of the most successful seismic discriminants proven so far is the classical comparison of body wave magnitude (m_b) to surface wave magnitude (M_S) (Basham, 1969; Lieberman and Pomeroy, 1969; Marshall, 1970; Stevens and Day, 1985), which exploits the observation that for a given m_b, explosions have a significantly smaller M_S than do earthquakes. This observation implies that explosive sources are richer in high frequency energy than are earthquakes for a given long-period energy level and is attributed, in part, to the differences in characteristics temporal and spatial source dimensions between the two source types. Savino *et al.* (1971), Aki et al. (1974), and Müller (1973) find that explosions exhibit characteristics of an impulsive source. Empirical explosion source models developed by Haskell (1967), and Müller and Murphy (1971) yield source time functions with rise times that are only fractions of second in length. Aki (1967), Brune (1970), and Marshall (1970) find that earthquake source functions, in contrast, are best-modeled as ramps or step functions with com-

bined duration and rise times greater than 1 sec. Dreger and Helmberger (1991a) found that even moderate-sized earthquakes ($M_L \sim 5.2$) have source durations greater than 1 sec. Stevens and Day (1985) conclude from numerical modeling experiments that the difference between earthquake and explosion source spectra is only partially responsible for explaining m_b:M_S observations. They also cite focal mechanism, near-source elastic properties, and *pP*-interference effects as contributing factors to the separation of populations with this type of discriminant.

The drawback to the m_b:M_S method is the threshold at which teleseismic surface wave magnitudes can be determined and the apparent convergence of populations at small magnitudes. Lieberman and Pomeroy (1969) found the surface wave detection level for earthquakes to be $m_b > 4.3$ and for explosions to be $m_b > 4.8$, but found that the populations converged below $m_b = 5.0$ for discrimination purposes. Evernden *et al.* (1971) suggest that with high-dynamic-range digital instruments, surface waves from earthquakes with $m_b > 4.0$ (which corresponds roughly to a $m_b = 5.0$ explosion) can be measured to 6000 km to 7000 km—distances at which well-dispersed 20-sec surface waves can be measured. Broadband, high-dynamic-range seismic stations, such as those in the IRIS network achieve this observational capability.

Below these threshold levels the surface wave signals are within the noise level and analogous discriminants using regional phases must be employed. Evernden *et al.* (1971), Lambert and Alexander (1971), and Peppin and McEvilly (1974) found that they could distinguish between source types on the basis of regional P_n amplitude (or $m_{b[P_n]}$) to regional airy phase Rayleigh wave amplitude (or magnitude) comparisons for events down to $m_{b(P_n)} = 3.6$ to 4.0—the detection threshold for explosion generated surface waves.

Two significant advances in observational seismology occurred since these studies. One is the large-scale upgrade and augmentation of seismic networks with broadband, high dynamic range instruments. The other is the increased sophistication in source parameterization of earthquakes and explosions in terms of the excitation of Green's functions and the seismic moment tensor solutions (Dziewonski *et al.* 1981), which more precisely quantify seismic sources. With several three component, broadband stations it is feasible to invert for the source function using regional body waves (Dreger and Helmberger, 1990; 1992), surface waves (Kanamori and Given, 1981; Thio and Kanamori, 1992; Patton, 1988) or a combination of the two wave types (Zhao and Helmberger, 1993). M_0 should better reflect the long-period source characteristics of a source than does M_S, so that its use should improve discriminants that make use of long-period seismic phases.

We re-examine the utility of short-period versus long-period energy measures in the context of regional seismic records. Figure 1 displays the study area, which includes central and southern California, western Nevada and northern Baja, Mexico. Waveform data is presented in this paper for the events shown in the figure (stars). This region is unique in that there is a large amount of natural seismicity, as well as that of Nevada Test Site (NTS) explosions and their aftershocks. The large number of seismic networks monitoring this region has created a wealth of data useful for discrimination studies.

With M_0 serving as a long-period energy measure, we employ the classical local magnitude, M_L, (Richter, 1935; 1958) as a measure of short-period energy. M_L is computed from the peak horizontal displacements on a Wood–Anderson

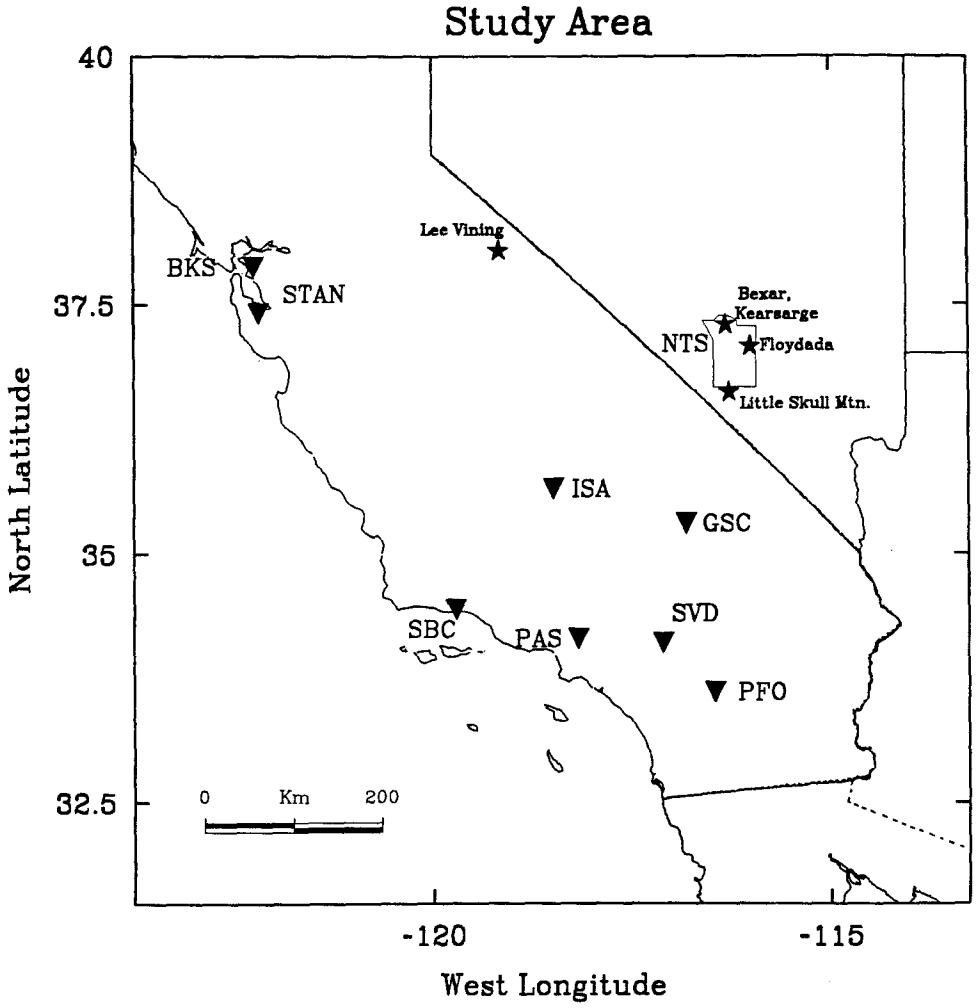

FIG. 1. Map showing the study area. Broadband stations used to determine M_0 and M_L for 1988 + events are shown with triangles. Events shown in this study are denoted by stars.

torsion instrument, which is a high pass filter peaked around 1.0 sec. Teleseismic P-wave phases measured to determine body-wave magnitudes are typically of the same period, so M_L, too, can be considered a fair measure of the short-period source spectrum. There are several advantages of using M_L. One is that it is a simple measurement to make and is easy to obtain to very small magnitudes. Secondly, it is a routine source quantification used by many seismic networks. We will make use of M_L magnitudes from several network catalogs. One drawback to measuring M_L is that it is not determined from a particular seismic phase. Normally it is a measure of shear-wave amplitude, but depending on distance and source spectrum for extreme circumstances, a P-wave or surface wave may be the largest amplitude phase on a short-period record.

From visual inspection of broadband recordings of regional earthquakes and explosions it is apparent that these two source types show distinctly different spectral content. Figure 2a compares records of the explosion Kearsarge (the 150 kt, m_b = 5.5, Joint Verification Event detonated at Pahute Mesa) with two

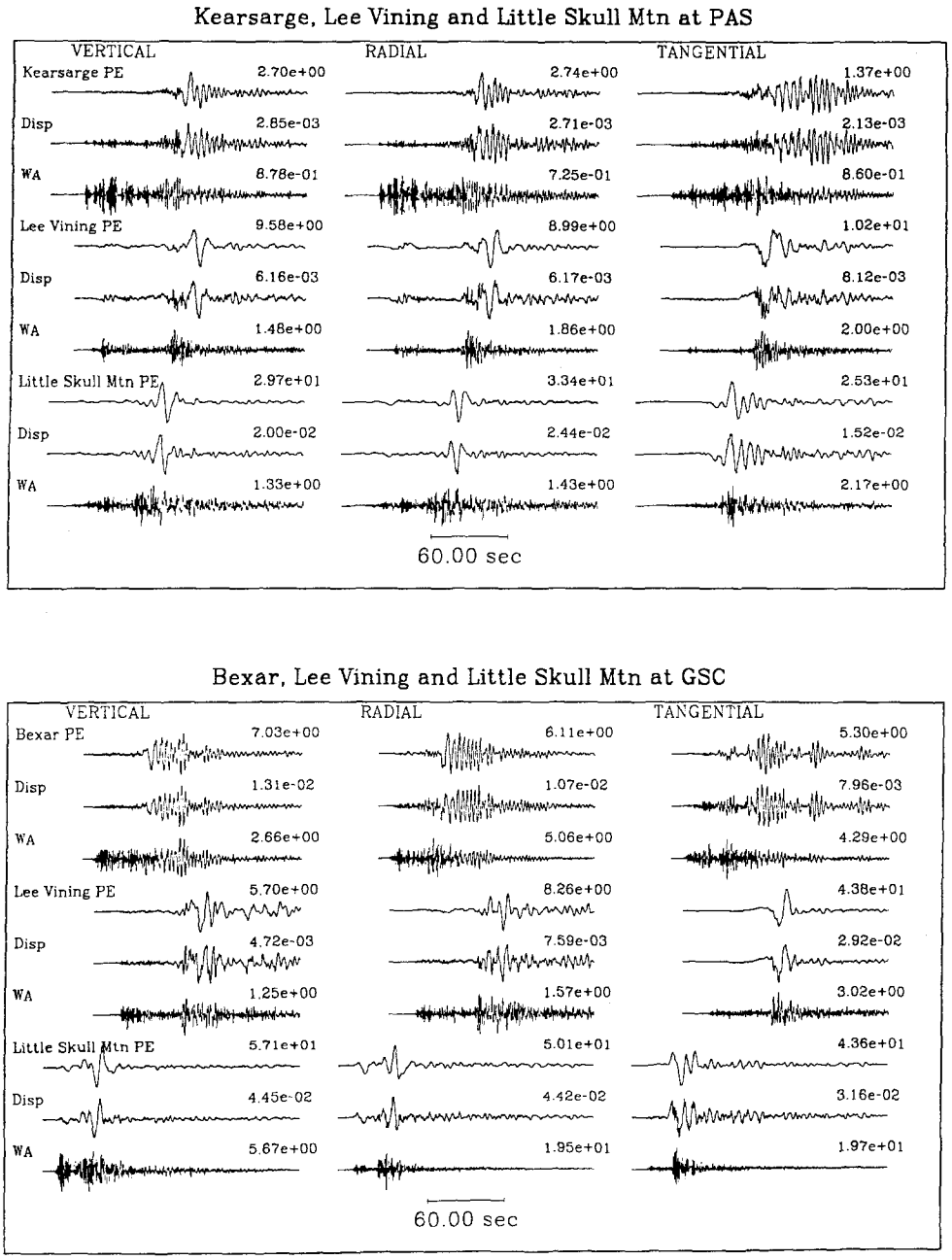

FIG. 2. (a) Broadband displacement (*middle trace*) records of the JVE event Kearsarge and the Lee Vining and Skull Mountain earthquakes recorded at PAS and played out with long-period (*top trace*) and short-period (*bottom trace*) instruments. (b) Analogous plot for the explosion Bexar and the Lee Vioning and Skull Mountain earthquakes recorded at GSC.

earthquakes: Lee Vining (10/24/90, $m_b = 5.0$) and Little Skull Mountain (6/29/92, $m_b = 5.7$). The three events, all recorded digitally at Pasadena, California (PAS), have roughly the same epicentral distance (see Fig. 1). For each event the broadband displacement records are displayed (*middle trace*), as well as the displacements convolved with a Press—Ewing 30 to 90 (PE) long-

period instrument (*top trace*) and with a Wood—Anderson short-period (WA) instrument (*bottom trace*). Peak amplitudes are to the right of each trace. For Kearsarge, the ratio of peak short-period (WA trace) to long-period (PE trace) amplitude is 0.325, 0.265, and 0.625 for the vertical, radial, and tangential component, respectively. On the long-period tangential component, no fundamental Love wave is apparent; only later arriving, higher frequency, higher mode waves (L_g and possibly multi-pathing crustal waveguide surface waves) are evident. The absence of a Love wave is also evidence of an isotropic source because explosions, in the absence of tectonic strain release, do not generate long-period *SH* waves. For Lee Vining the ratio of peak short-period to long-period amplitude is 0.152, 0.223, and 0.210 for the vertical, radial, and tangential components. The tangential component also has a large fundamental mode Love wave. For Little Skull Mountain the ratio of peak short-period to long-period amplitude is 0.0451, 0.0433, and 0.0872 for the vertical, radial, and tangential components. Again, a large Love wave is observed. Of these three events, the explosion has the largest short-period to long-period amplitude ratio for each component.

Figure 2b shows an analogous plot of seismograms recorded at the digital station Goldstone, California (GSC), for the explosion Bexar (m_b = 5.6 and detonated within a kilometer of the Kearsarge shot point) and the two earthquakes of Figure 2. As with Kearsarge, little or no long-period Love wave is evident on the tangential component; only shorter period crustal waveguide surface waves are visible. The ratio of peak short-period to long-period amplitude for Bexar is 0.379, 0.794, and 0.794 for vertical, radial, and tangential component, respectively. For Lee Vining the ratio of peak short-period to long-period amplitude is 0.221, 0.189, and 0.0694 for the vertical, radial, and tangential components. For Little Skull Mountain the respective ratios are 0.0989, 0.394, and 0.455. Again, the explosion has the largest short-period to long-period amplitude ratio for each component.

Another comparative difference between the explosions and earthquakes in these figures is the spectral content of the Rayleigh waves. The explosion Rayleigh waves exhibit large, relatively short-period (3 to 8 sec) "ringing" or coda waves after the Airy phase, whereas the earthquakes display primarily the dominant long-period Airy phase. This effect is believed to be a depth dependent phenomena. Kafka (1990) found, in a study of New England earthquakes and quarry blasts, that shallow events produce larger short-period (0.4 to 2.5 Hz) R_g waves than do deeper events. Such Rayleigh wave information is useful as a depth discriminant to help distinguish source types.

These sets of records corroborate the observation that explosions are richer in short-period energy relative to long-period energy as compared to earthquakes. Events recorded at both PAS and GSC have been plotted in order to illustrate that this observation is path independent. Of the network shown in Figure 1, only PAS and GSC recorded the Lee Vining event. We will show, using a large data set, that this spectral difference becomes even more evident after applying propagational corrections and can be used as an effective regional discriminant.

Data Analysis and Results

We compiled seismic moments (M_0) and local magnitudes (M_L) for NTS explosions and earthquakes throughout the western United States and northern Baja California, Mexico from many sources. M_L values were taken from the CIT

and Berkeley catalogs, and from the Northwestern Mexico Seismic Network (Vidal and Munguia, 1991). For recent events (1988 to 1992) in Nevada and the California-Nevada Border region, M_L's were determined from the array of eight broadband stations shown in Figure 1. To calculate these M_L's, an attenuation curve developed by Kanamori *et al.* (1992) was used. All the M_L's used were determined in essentially the same fashion.

The seismic moments collected for this study, however, were determined through a variety of means. Dreger and Helmberger (1990, 1991a, 1991b, 1992), Ma and Kanamori (1991), and Zhao and Helmberger (1993) inverted local and regional broadband waveforms to obtain source parameters, including moment. Cohn et al. (1982) forward modeled near-field broadband records to determine earthquake moments. Moments determined from combined regional phase (P_{nl}) and teleseismic body waves (P and SH) studies were also gathered. Bent and Helmberger (1991) used a combination of forward modeling comparative amplitude ratios to estimate moments for historical southern California. We also included moments and local magnitudes compiled from various source studies for historical western United States earthquakes (Doser and Smith, 1989; Doser, 1990).

Moments from several short-period array source studies were incorporated into our data set. Mori and Frankel (1990) obtained moment estimates from deconvolved displacement pulses. Employing the method of Brune (1970), several studies calculated M_0 from the low-frequency amplitude of shear-wave spectra (Johnson and McEvilly, 1974; Fletcher *et al.*, 1984; Frankel, 1984; Vidal and Munguia, 1991).

Surface wave moments were also obtained from a variety of sources. Thio and Kanamori (1992) obtained source parameters from broadband TERRAscope data for earthquakes throughout southern California for a wide range of magnitudes. Their inversion method uses both Rayleigh wave and Love wave spectra and employs the technique of Kanamori and Given (1981). Patton and Zandt (1991) determined moment tensor solutions for earthquakes throughout the western U.S. using a linear moment inversion scheme developed for Rayleigh wave spectra by Romanowicz (1982) and extended to Love wave spectra by Patton (1988). Wyss and Brune (1968) determined moments from Love wave spectra for central California events.

Table 1 is a list of the local magnitudes and log-moments for earthquakes for which source parameters were determined from broadband data. It includes all available data from the studies by Dreger and Helmberger (1990, 1991a, 1991b, 1992), Ma and Kanamori (1991), and Thio and Kanamori (1992).

Table 2 lists the local magnitudes and log-moments for explosions cited in this study. Seven explosion moments were determined from near-field observations (Aki *et al.*, 1974; Helmberger and Hadley, 1981; Stump and Johnson, 1984; and Johnson, 1988), although most were obtained from surface wave studies. Stevens (1986) calculated spectral moments from Rayleigh wave spectra for large NTS explosions Given and Mellman (1986) performed moment tensor inversions of large NTS blasts, too, using the path structures developed by Stevens (1986). They used Rayleigh wave and Love wave spectra to solve for the isotropic source as well as a double-couple source associated with tectonic release. The data sets for these last two studies overlap substantially. The moment values were found to be similar, so that for events for which two moments were available, the Stevens' (1986) moment was used.

TABLE 1

EARTHQUAKES WITH MOMENTS DETERMINED USING BROADBAND DATA

Date	M_L	log(M_0)	Event	Date	M_L	log(M_0)	Event
88/06/10	5.4	17.11[a]	Gorman	92/03/03	3.4	14.49[a]	Walker Pass
88/06/26	4.6	15.78[d]	Chino	92/03/04	4.2	15.14[a]	San Clemente
88/06/27	5.5	16.77[c]	San Juan Botista	92/03/05	3.8	14.59[a]	Bakersfield
88/07/06	3.7	14.88[d]	Chino A.S.	92/04/10	3.4	14.60[a]	Borrego
88/12/03	4.9	16.38[b]	Pasadena M.S.	92/04/15	3.4	14.00[a]	Lytle Creek
11:49:	2.1	12.41[b]	Pasadena A.S. 1	92/04/23	4.6	15.49[a]	Joshua Tree F.S.
12:08:	2.0	13.02[b]	Pasadena A.S. 3	92/04/23	6.1	18.29[a]	Joshua Tree M.S.
12:13:	2.4	13.02[b]	Pasadena A.S. 4	13:58:	4.1	15.01[a]	Joshua Tree A.S. 1
12:15:	1.6	12.40[b]	Pasadena A.S. 5	22:55:	3.8	14.54[a]	Joshua Tree A.S. 2
13:36:	1.8	12.09[b]	Pasadena A.S. 6	23:52:	3.8	14.54[a]	Joshua Tree A.S. 3
14:46:	1.9	11.88[b]	Pasadena A.S. 7	92/04/24	3.5	14.37[a]	Joshua Tree A.S. 4
88/12/04	2.0	12.24[b]	Pasadena A.S. 8	18:06:	3.7	14.52[a]	Joshua Tree A.S. 5
88/12/08	2.2	12.64[b]	Pasadena A.S. 9	18:20:	3.7	14.61[a]	Joshua Tree A.S. 6
89/01/19	5.0	16.51[a]	Malibu	92/04/25	3.7	14.73[a]	Joshua Tree A.S. 7
89/02/18	4.3	15.34[e]	Upland	18:56:	4.4	15.05[a]	Joshua Tree A.S. 8
89/08/08	5.3	16.41[c]	Los Gatos	92/04/26	3.7	14.27[a]	Joshua Tree A.S. 9
89/10/18	7.0	19.48[c]	Loma Prieta	6:26:	4.2	15.69[a]	Joshua Tree A.S. 10
90/02/28	3.7	14.65[e]	Upland F.S.	17:21:	4.3	15.39[a]	Joshua Tree A.S. 11
90/02/28	5.2	17.40[e]	Upland M.S.	92/04/27	4.2	15.41[a]	Joshua Tree A.S. 12
90/03/01	4.7	15.70[e]	Upland A.S.	92/04/28	3.7	14.90[a]	Joshua Tree A.S. 13
90/03/02	4.6	15.60[e]	Upland A.S.	11:33:	3.8	15.12[a]	Joshua Tree A.S. 14
90/04/17	4.6	15.78[e]	Upland A.S.	92/04/30	3.7	14.70[a]	Joshua Tree A.S. 15
90/10/24	5.0	16.70[g]	Lee Vining	92/05/01	3.8	14.71[a]	J. T. A.S. 16
90/12/17	3.7	14.38[a]	Big Bear I	92/05/02	4.1	14.64[a]	J. T. A.S. 17
90/12/18	3.7	15.04[a]	White Wolf Fault	19:10:	3.4	14.35[a]	J. T. A.S. 18
91/05/20	3.7	14.48[a]	San Jacinto I	92/05/04	4.0	15.04[a]	J. T. A.S. 19
91/05/20	3.7	14.20[a]	San Jacinto II	16:19:	4.8	16.19[a]	J. T. A.S. 20
91/06/28	5.4	17.41[f]	Sierra Madre	92/05/06	4.5	15.87[a]	J. T. A.S. 21
15:37:	3.9	14.61[f]	S. Madre A.S.	92/05/12	4.4	15.60[a]	J. T. A.S. 22
17:00:	4.3	15.60[f]	S. Madre A.S.	92/05/18	3.5	14.39[a]	J. T. A.S. 23
91/06/29	4.0	14.60[a]	Mojave	15:44:	4.9	16.10[a]	J. T. A.S. 24
91/07/06	3.8	14.59[f]	S. Madre A.S.	92/06/11	4.3	15.29[a]	J. T. A.S. 25
91/10/12	4.0	15.04[a]	Blue Cut	92/05/31	3.2	13.78[a]	Lenwood Flat I
91/10/27	3.4	14.26[a]	San Jacinto	92/05/31	3.5	14.28[a]	Lenwood Flat II
91/12/03	5.4	16.72[g]	San Miguel	92/06/28	3.7	14.29[a]	Landers A.S.
91/12/04	4.2	14.95[a]	Julian	92/06/29	5.4	16.85[a]	Landers A.S.
91/12/04	4.0	14.62[a]	Big Bear II	14:41:	4.4	16.90[a]	Landers A.S.
92/02/17	3.5	14.66[a]	Coso	16:01:	5.2	17.16[a]	Landers A.S.
92/02/19	4.0	14.85[a]	Coso I	92/06/29	5.6	17.40[c]	Little Skull Mtn
92/02/19	3.7	14.41[a]	Coso II	92/06/29	3.7	14.66[a]	La Canada
92/02/21	3.7	15.30[a]	Coso	92/06/30	4.7	15.83[a]	Landers A.S.
92/02/22	3.9	14.28[a]	Coso	21:49:	4.3	15.87[a]	Landers A.S.

[a]Thio and Kanamori, 1992; [b]Ma and Kanamori, 1991; [c]Zhao and Helmberger, 1993; [d, e, f, g]Dreger and Helmberger, 1990, 1991a, 1991b, 1992.

Time domain surface wave moments of explosions were also included in this study. Woods and Harkrider (1993) determined moments from the peak to peak amplitude (PPA) of the dominant Airy phase of the Rayleigh wave for NTS explosions. With their technique, moment is determined from the ratio of the observed PPA to that of a synthetic seismogram with a given input moment. Figure 3 plots comparisons of observed versus modeled vertical Rayleigh waves for the 55 station network used in their study. Data from representative Pahute

TABLE 2

EXPLOSIONS IN THIS STUDY

Date	M_L	$\log(M_0)$	Event	Date	M_L	$\log(M_0)$	Event
57/09/19	4.25	14.30[a]	Rainier	70/03/19	4.05	13.65[g]	Jal
61/12/03	3.91	13.86[a]	Fisher	70/03/23	5.29	15.73[g]	Shaper
62/06/27	4.63	14.55[g]	Haymaker	70/03/26	6.17	17.72[c]	Handley
65/02/16	4.21	13.98[g]	Merlin	70/05/01	4.18	14.35[h]	Beeblam
65/03/03	5.04	15.41[g]	Wagtail	70/05/05	4.82	14.70[g]	Mintleaf
65/04/14	4.23	14.02[g]	Palanquin	70/05/15	5.00	15.19[g]	Cornice
65/05/12	3.91	13.84[g]	Buteo	70/05/21	3.60	13.23[g]	Manzanas
66/04/25	4.69	14.90[g]	Pinstripe	70/05/21	5.00	14.98[g]	Morrones
66/04/14	5.02	15.39[g]	Duryea	70/05/26	4.63	14.60[g]	Hudsonmoon
66/05/05	4.04	14.24[g]	Cyclamen	70/05/26	5.20	15.56[g]	Flask
66/05/13	5.01	15.75[g]	Piranha	71/06/19	4.20	13.83[g]	Embudo
66/06/02	4.98	15.73[g]	Piledriver	71/06/23	4.50	14.45[g]	Laguna
66/06/25	4.33	14.13[g]	Vulcan	71/06/29	4.90	14.64[g]	Harebell
66/06/30	5.90	16.49[g]	Halfbeak	71/10/29	4.10	14.03[g]	Pedernal
66/12/20	6.07	16.98[g]	Greeley	71/10/08	4.10	14.02[g]	Cathay
67/02/08	4.09	13.82[g]	Ward	72/04/19	4.20	13.73[g]	Longchamps
67/02/23	3.89	13.81[g]	Persimmon	72/05/19	4.48	14.66[g]	Monero
67/04/07	3.97	13.76[h]	Fawn	72/10/03	4.40	13.93[g]	Delphinium
67/04/21	3.83	13.51[h]	Effendi	73/06/06	5.68	16.78[e]	Almendro
67/04/21	3.89	13.72[h]	Chocolate	75/05/14	5.86	16.50[e]	Tybo
67/05/23	5.57	16.46[e]	Scotch	75/06/19	5.74	16.58[e]	Mast
67/06/26	4.54	14.42[g]	Midimist	75/06/26	5.95	16.96[g]	Camembert
79/06/20	3.92	13.91[h]	Chess	84/05/01	5.10	15.76[g]	Mundo
79/09/06	5.30	16.16[d]	Hearts	84/05/31	5.30	15.89[g]	Caprock
79/09/26	5.20	15.98[d]	Sheepshead	84/06/20	4.40	14.48[g]	Duoro
79/11/29	3.89	13.66[h]	Backgammon	84/07/25	5.30	15.52[g]	Kappeli
80/03/08	3.89	13.43[h]	Norbo	84/08/02	4.30	14.28[g]	Correo
80/04/26	5.10	15.91[e]	Colwick	84/08/30	4.50	14.52[g]	Dolcetto
80/04/30	5.10	15.61[g]	Pyramid	84/09/13	4.80	15.01[g]	Berton
80/07/25	5.10	16.10[d]	Tafi	84/11/10	4.30	14.21[g]	Villita
80/10/31	4.50	14.77[g]	Minersiron	84/12/09	5.10	15.63[g]	Egmont
81/01/15	5.20	15.79[g]	Baseball	84/12/15	5.00	15.63[g]	Tierra
81/06/06	5.40	15.87[f]	Harzer	85/03/15	4.60	14.77[g]	Vaughn
81/11/12	5.00	15.61[g]	Rousanne	85/03/23	5.00	15.31[g]	Cottage
82/01/28	5.30	16.08[g]	Jornada	85/04/02	5.40	16.12[g]	Hermosa
82/02/12	5.00	15.95[g]	Molbo	85/04/06	4.50	14.86[g]	Misty-rain
82/02/12	5.00	15.90[g]	Hosta	85/06/12	5.10	15.85[g]	Salut
82/04/17	4.40	14.35[g]	Tenaja	85/07/25	5.20	15.73[g]	Serena
82/04/25	5.00	15.79[g]	Gibne	85/12/05	5.20	15.56[g]	Kinibito
82/05/07	5.20	15.76[g]	Bouschet	85/12/28	5.00	15.57[g]	Goldstone
82/06/24	5.20	15.96[g]	Nebbiolo	86/03/22	5.10	15.46[g]	Glencoe
82/07/29	4.10	14.45[g]	Monterey	86/04/10	4.50	14.78[g]	Mightyoak
82/08/05	5.40	16.16[g]	Atrisco	86/04/22	5.00	15.71[g]	Jefferson
82/09/02	3.50	13.23[g]	Cerro	86/05/21	4.00	13.96[g]	Panamint
67/08/31	4.73	14.46[g]	Doormist	75/10/24	4.86	14.80[g]	Huskypup
67/09/21	3.87	13.51[g]	Marvel	75/10/28	6.08	17.03[g]	Kasseri
67/09/27	5.66	16.32[e]	Zaza	76/02/12	6.12	17.00[g]	Fontina
68/01/19	5.74	16.83[g]	Faultless	76/02/26	5.86	16.79[e]	Cheshire
68/03/12	3.96	14.28[g]	Buggy	76/03/09	5.83	16.79[e]	Estuary
68/04/26	6.09	17.24[g]	Boxcar	76/03/17	5.77	16.52[e]	Pool
68/04/24	5.06	14.85[g]	Hudsonseal	77/04/05	5.20	16.01[e]	Marsilly
68/11/04	4.46	14.57[g]	Crew	77/04/27	4.90	15.62[g]	Bulkhead
68/12/19	6.14	17.35[g]	Benham	77/05/25	5.00	15.52[g]	Crewline
69/02/12	4.81	14.63[g]	Cypress	77/11/09	5.40	16.27[e]	Sandreef
69/05/07	5.68	16.42[e]	Purse	77/12/14	5.30	16.22[e]	Farallones

TABLE 2—*Continued*

Date	M_L	log(M_0)	Event	Date	M_L	log(M_0)	Event
69/09/16	6.19	16.82[b]	Jorum	78/03/23	5.30	16.02[d]	Iceberg
69/10/08	5.50	16.19[c]	Pipkin	78/04/11	5.10	15.89[d]	Backbeach
69/10/29	4.40	13.55[g]	Cruet	78/07/12	5.20	15.75[g]	Lowball
6910/29	4.60	13.97[g]	Pod	78/08/31	5.30	15.92[d]	Panir
69/10/29	5.50	15.79[g]	Calabash	78/09/13	4.40	14.55[g]	Diablohawk
70/20/11	4.67	14.77[g]	Diamamist	78/09/27	5.30	16.15[d]	Rummy
70/02/25	4.60	14.89[g]	Cumarin	78/11/02	4.23	14.36[h]	Emmenthal
70/02/26	4.80	14.65[g]	Yannigan	78/11/18	5.00	15.30[g]	Quargel
70/03/06	4.20	13.57[g]	Cyathus	78/12/16	5.20	16.40[c]	Farm
70/03/06	4.10	13.09[g]	Arabis	79/02/08	5.20	15.80[g]	Quinella
79/06/11	5.30	16.13[d]	Pepato	84/03/31	4.20	13.71[g]	Agrini
82/09/23	4.60	14.82[g]	Huronlanding	86/06/05	5.30	15.58[g]	Tajo
82/09/23	4.60	14.88[g]	Frisco	86/06/25	5.30	15.61[g]	Darwin
82/09/29	3.80	13.98[g]	Borrego	86/07/17	5.20	15.08[g]	Cybar
82/11/12	4.10	13.92[g]	Seyval	86/07/24	4.70	14.40[g]	Cornucopia
82/12/10	4.40	14.56[g]	Manteca	86/09/30	5.40	15.72[g]	Labquark
83/03/26	4.90	15.44[g]	Cabra	86/10/16	5.30	15.77[g]	Belmont
83/04/14	5.20	15.59[g]	Torquoise	87/04/18	5.30	15.77[g]	Delamar
83/05/26	4.30	14.26[g]	Fahada	87/04/30	5.30	15.88[g]	Hardin
83/06/09	4.30	14.29[g]	Danablu	87/06/18	4.00	13.90[h]	Brie
83/09/01	5.30	15.77[f]	Chancellor	87/10/23	5.40	15.31[g]	Borate
83/09/22	4.00	13.90[g]	Techado	88/04/07	3.60	12.75[h]	Abliene
83/12/16	4.80	15.22[g]	Romano	90/06/21	4.30	13.91[h]	Austin
83/05/05	4.20	14.26[g]	Crowdie	91/08/15	4.00	14.10[h]	Floydada
84/02/15	4.50	14.78[g]	Milagro	92/09/18	4.00	14.02[h]	Hunterstrophy
84/03/01	5.30	15.85[g]	Tortugas	92/09/23	4.41	14.27[h]	Divider

[a]Aki *et al.* 1974; [b]Helmberger and Hadley, 1981; [c]Stump and Johnson, 1984; [d]Given and Mellman, 1986; [e]Stevens, 1986a; [f]Johnson, 1988; [g]Woods and Harkrider, 1993; [h]This study.

Mesa NTS explosions, with little or no tectonic release, are the upper, darker traces. The synthetics seismograms were generated with a step moment source buried at 0.6 km, a typical shot depth. Many of the path structures used were taken from the Stevens (1986) study. Other paths were determined by inverting Rayleigh wave dispersion data. It can be seen that the waveform fits are good, in that dispersion and amplitude are both well-modeled. The correlation between moments obtained by this time domain moment and a more standard spectral scheme performed on a 108 event subset of this study is very good (see Woods and Harkrider, 1993), implying that this time domain moment method yields accurate, robust moment measurements. Using this method we obtained moments for other small NTS events.

Figure 4a displays M_L versus log Moment (*N-m*) plotted for 299 earthquakes and 178 explosions. Solid symbols represent earthquakes, whereas open symbols and crosses represent NTS explosions. Moments determined from near-field body wave studies are plotted as circles. Earthquake moments determined from surface wave studies and body wave studies are represented by triangles and diamonds, respectively. Explosion moments determined from surface source studies are denoted by stars (Given and Mellman, 1986), squares (Stevens, 1986), and crosses (Woods and Harkrider, 1993). This figure shows how well this discriminant works. There is a significant separation of earthquakes and explosions, with no real overlap of the two populations. This discriminant also

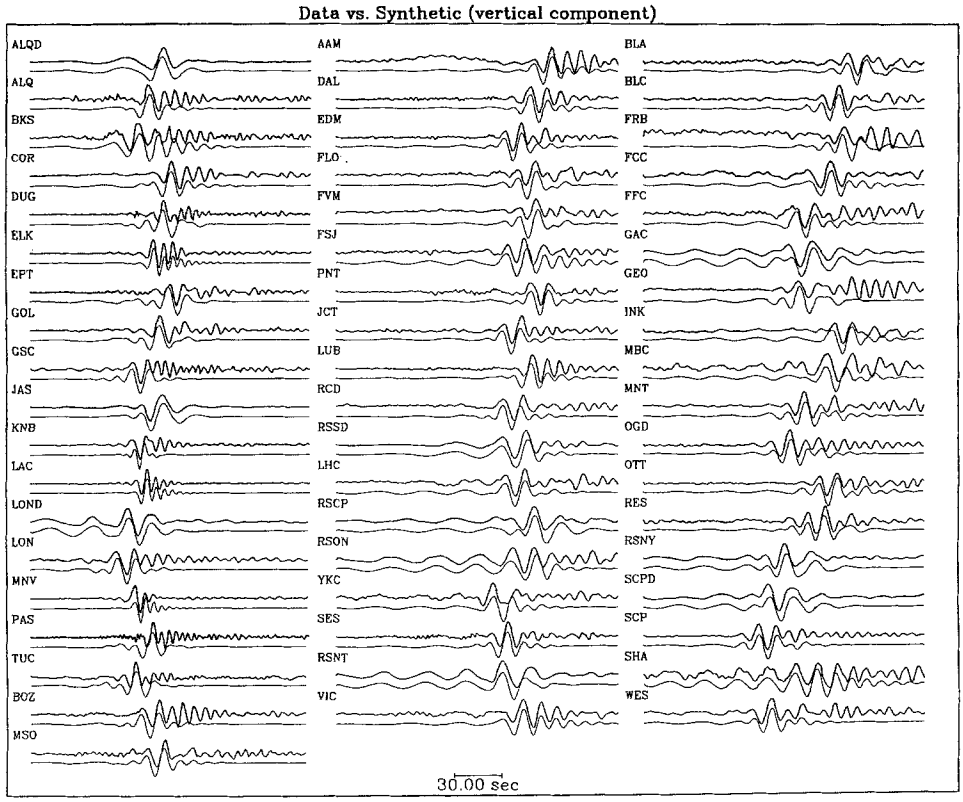

FIG. 3. Comparison of synthetic and observed fundamental Rayleigh waves for a regional network from which seismic moments were determined. The data are the upper, darker traces. The records chosen came from an ensemble of high-SNR Pahute Mesa events with little or no tectonic release. The synthetics were generated with a step moment isotropic source buried at 0.6 km.

works at all scales, with explosions and earthquakes following their respective scaling laws over a wide range of magnitudes and moments; for earthquakes this is true over seven and half orders of magnitude. It should be noted that the earthquakes with a $\log(M_0)$ below 13.0 were determined from local stations ($D < 75$ km) and would not be detectable at regional distances. They are included here only to show the continuity of the linear scaling relationship between M_L and $\log(M_0)$ for earthquakes.

Figure 4b is a blow-up of the portion of Figure 4a containing explosion data. It is important to note when examining these two plots that the data are taken from a number of sources. M_L's were determined from different networks and the moments were calculated in a variety of ways. Yet a distinct separation of the two populations is still obtained. There is one anomalous explosion, Buggy ($M_L = 3.96$, $\log(M_0) = 14.28$), which lies very close to the earthquake population. This was a Plow Shares event in which four nuclear charges with an announced combined yield of 5.4 kt were detonated. We would expect that a multiple-source event like this one would display characteristics similar to a distributed earthquake source, i.e., it should be enriched in long-period energy relative to a point source explosion of the same yield.

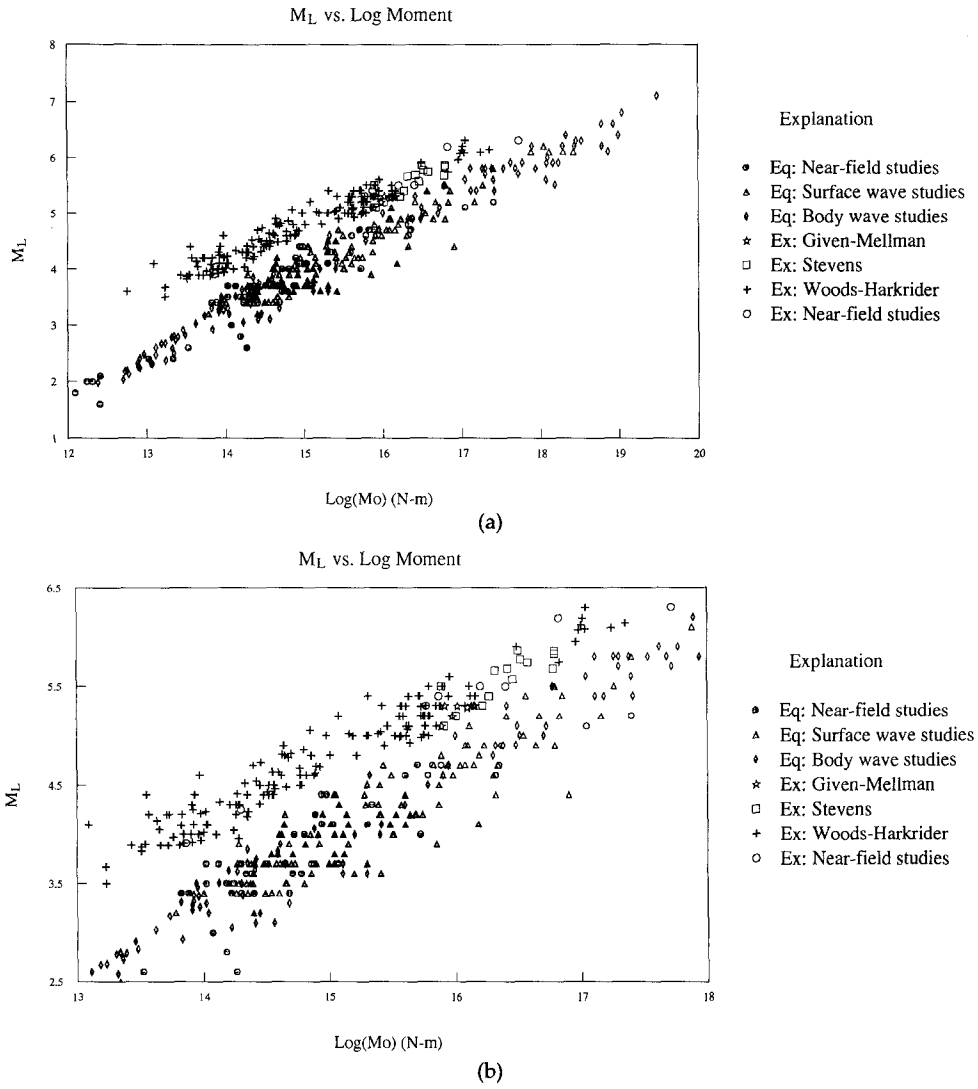

FIG. 4. (a) M_L versus log M_0 for 299 earthquakes (solid symbols) and 178 explosions (open symbols and crosses). Circles are moments from near-field source studies. Triangles are surface wave moments and diamonds are body wave moments. Explosion moments determined from surface waves are shown as stars (Given and Mellman, 1986), squares (Stevens, 1986a) and crosses (Woods and Harkrider, 1993). (b) Blow-up of that part of the plot that contains explosions.

DISCUSSION AND CONCLUSIONS

The M_L:M_0 criterion appears to be a robust method to discriminant regional seismic events. For a given moment, the M_L of an explosion is more than 0.5 units larger than that of an earthquake. This difference can be attributed to M_L being a short-period (1 Hz) energy measurement, whereas the moment is determined from long-period body wave phases (period > 4 sec) and Rayleigh waves (10 to 40 sec).

There are several explanations for the observed difference in short-period: long-period spectral character between earthquakes and explosions. Earth-

quakes tend to be asperity-driven distributed sources, as opposed to explosions that can more aptly be modeled as point-sources with impulsive time functions. Dreger and Helmberger (1991a) showed that broadband seismograms from small local earthquakes ($4.0 < M_L < 5.0$) can be modeled as distributed finite sources rather than as point-sources. Such distributed slip time functions will generally result in reduced high-frequency spectra relative to a point-source step moment. It is possible that even very small earthquakes ($M_L < 4$) behave similarly. Another possible reason that this discriminant works at low magnitudes is that for small events the quantities being measured are the *P*-wave low frequency spectrum (M_L) and the *S*-wave low frequency spectrum (M_0), in which case, for explosions, the *S*-wave energy is predominantly generated by secondary *P* to *S* converted phases. If this is so, the moment should not be determined solely from *P*-wave information.

Spall effects may also be a cause of observed high-frequency ($0.15 \text{ Hz} < f < 2.0$ Hz) enrichment of explosion source spectra. Theoretical results (Day and McLaughlin, 1991) and various observational studies (Viecelli, 1973; Stump, 1985; Taylor and Randall, 1989; and Patton, 1990) conclude that spallation can be a significant contributor to short period energy, whereas Patton (1988) and Day *et al.* (1983) find no appreciable spall energy at periods greater than 8 sec. Spall energy would tend to increase M_L measurements.

This discriminant is only limited by the detection threshold capability of long-period data, as the two populations do not converge at small magnitudes. This observation implies that the convergence in the M_S:m_b ratio for small magnitude events seen in some previous studies is due to approaching the effective signal to noise level for measuring surface amplitudes. Previous studies relied on data recorded on lower grade (usually analog) instruments that did not have the record capabilities of modern, high dynamic range, digital seismometer systems. Modern data combined with digital processing techniques increases the resolution of long-period transient signals. Figure 5 shows the Yucca Flat blast Floydada recorded at four TERRAscope stations (epicentral distances being between 200 and 400 km), played-out with PE and WA instruments. The amplitudes indicate that these signals would not be discernible on the actual analog instruments. M_L for this event is 4.0 and its log moment is 14.20. Assuming it is a shallow explosion above the water table, the yield can be inferred to be less than 10 kt from the moment-yield scaling relationships determined for NTS by Woods and Harkrider (1993). Were it detonated in hard rock below the water table, it would correspond to a 2 kt kiloton explosion. We estimate that were this event 2.5 times lower in yield it would still be possible to obtain its moment, yielding a magnitude threshold of $M_L > 3.6$ for explosions.

Low SNR seismograms also may be phase match filtered (Herrin and Goforth, 1977; Stevens, 1986a) in order to retrieve the signal of very small events for spectral amplitude estimates. However, there is some debate on the accuracy of using this method, see Der (1986) and Stevens (1986b) for a discussion of this problem. Employing one or another means of time domain measurements in order to obtain the seismic moment avoids such problems.

Simple tiome domain moment measurements included in this study are straightforward and can be directly applied to historical analog data sets in order to establish earthquake M_L:M_0 curves for other regions. Because only peak amplitude measurements are necessary for such methods, the required

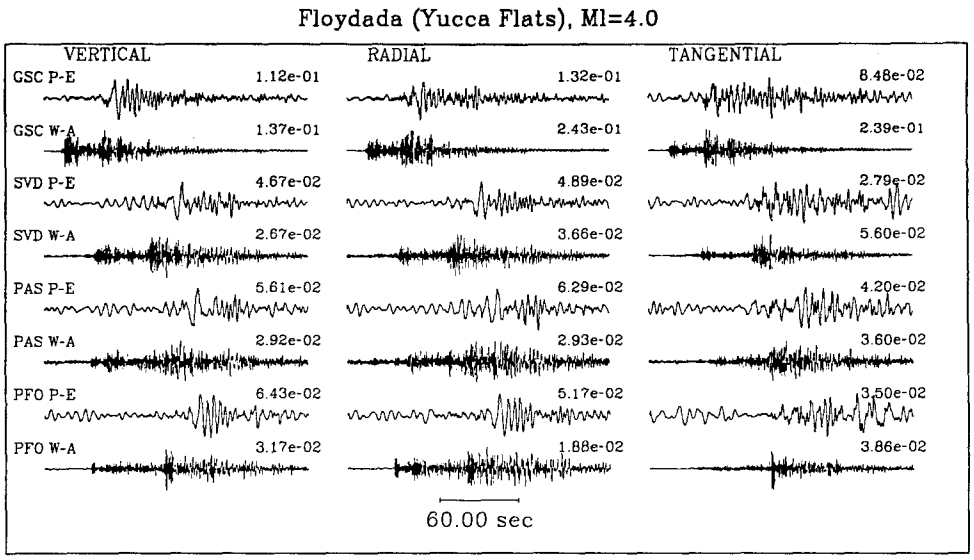

FIG. 5. A small Yucca Flat explosion, Floydada (M_L = 4.0), recorded at TERRA-scope stations and played out on Press—Ewing (long-period) and Wood—Anderson (short-period) instruments.

signal to noise ratio (SNR) effectively decreases, too. Time domain peak amplitude measurements are also less susceptible to noise contamination than are spectral amplitude measurements. The other parameter M_L is a simple time-domain measurement that can be made on the smallest detectable seismic sources. Modern source inversion techniques that make use of regional body wave phases (such as P_{nl} and S_{nl}) recorded at sparse regional networks also make for powerful moment determination tools as shown in studies using the TERRAscope broadband network (Dreger and Helmberger, 1992; Zhao and Helmberger, 1993).

A disadvantage to determining moment tensor solutions is that many methods require Green's functions in order to obtain accurate moments. However, with modern broadband, high dynamic range instrumentation it is quite feasible to use moderate-sized to small events to determine regional path structures. Zhao and Helmberger (1991) detail the forward modeling of P_{nl}, S_{nl}, and Rayleigh wave regional phases along a continental shield path. Dreger and Helmberger (1990) were able to forward model velocity structure using waveform data from small (m_b = 3.7 to 4.0) local events. Shallow crustal structure can also be inferred from the inversion of surface wave dispersion data generated by small, regional seismic sources (Saikia *et al.*, 1990) as well as in conjunction with teleseismic surface waves (Thio and Kanamori, 1991). These path structures need not be overly complicated or detailed. Dreger and Helmberger (1991b, 1992) found that they could model broadband regional body-wave phases from events located throughout Southern California and recorded at various TERRAscope stations with one relatively simple crustal model (with an underlying mantle half-space). Using their regional Green's functions in conjunction with a time-domain source inversion method yielded source parameter solutions consistent with other studies. Zhao and Helmberger (1993) extended this technique to include surface waves and found that this inversion scheme worked well with simple regional earth models as well.

An important point to address concerns the *a priori* source type assumptions made in determining the seismic moments. All earthquake moments were determined assuming either a double-couple source (for moment tensor and Green's function inversion methods) or a circular fault model (for corner frequency moment estimates). Most of the NTS explosion moments were determined by modeling the Rayleigh waves as being generated by a shallow, isotropic source excitation function in the absence of an azimuthally dependent radiation pattern. The Given and Mellman (1986) moments, however, were determined by inverting Rayleigh and Love wave spectra to obtain the isotropic and double-couple components of the moment tensor solution. An obvious problem with classifying events with respect to their M_L:M_0 ratio is that for an unidentified seismic event one doesn't know which source model to assume in order to estimate the moment. This point leads to the question, how distinguishable would the two populations be, had they all been treated as double-couple sources for moment estimation purposes? For a given seismic moment, the average radiation pattern amplitude (assuming absolute values) for Rayleigh waves generated by a predominantly strike-slip fault motion ($\sin 2\theta$ radiation pattern) is only slightly larger (by 10%) than that of an explosion. In this case one could still infer the source type from the moment estimate. For such strike-slip earthquakes, observations from all azimuthal quadrants (the four lobes of the $\sin 2\theta$ radiation pattern) will result in better constrained moment determinations.

The difficulty occurs in modeling the Rayleigh waves assuming a shallow source with a dip-slip orientation for which there is a singularity in the Green's function solutions. In this special case we would obtain a larger moment and the event's M_L:M_0 ratio would decrease toward the earthquake population. However, one can generally model and invert for earthquake sources that occur deeper than 3 km. When an event does not fit our regional Green's functions to some specified degree, we would assume it is shallow and model it as a vertical strike-slip earthquake. Thus, explosions would still discriminate as displayed above and shallow strike-slip earthquakes would still lie within the earthquake population. M_0 for a shallow dip-slip earthquake, however, may be underestimated and could potentially fall within the explosion population. In a monitoring environment we would have a problematic event, to which other discrimination criterion would need to be applied in order to identify it correctly.

Applying the M_L:M_0 ratio in conjunction with other discriminants would yield a more effective source identification scheme. Phase information (i.e., Rayleigh wave polarity) and Love wave data would be helpful in such cases because reversed polarity Rayleigh waves and/or large Love wave amplitudes are diagnostic of a double-couple source. A depth discriminant, based on the complexity and amplitude of the Rayleigh wave tail (coda) for example, would be useful for depth constraints to be placed on the moment tensor inversion of a source. In a related study Woods and Helmberger (1992) found that the ratio of short-period energy in the vertical component *Pnl*-wave train to that in the long-period surface wave train (summed over all three components) of regional seismograms also separates source populations, although it, too, suffers similar magnitude threshold limitations.

For very small events information from high-frequency ($f > 1$ Hz) phases may be needed to compliment the M_L:M_0 discriminant. Comparisons of L_g spectral amplitude levels for different bandwidths (in the 0.5 to 8 Hz range) have been

shown to effectively discriminate events with magnitudes down to $m_{b(P_n)} = 3.3$ (Murphy and Bennett, 1982; Taylor *et al.*, 1988). Although the M_L:M_0 discrimination threshold is slightly higher than this, the regional body wave phases and Rayleigh waves used in this method are not as susceptible to path "blockage" effects as is the L_g phase. Also, using relatively close-in stations for surface wave measurements, as it is possible to do with this method, path atteuation effects are minimized. The M_L:M_0 ratio discriminant would work well as a companion test, or check, for other, high-frequency, discrimination methods, particularly for events in the $3.5 < m_b < 4.5$ range for which teleseismic methods no longer work.

Because both source parameters used in this discrimination method can be obtained from a sparse broadband network, this discriminant can be applied throughout the world as more broadband stations similar to those of the IRIS network come on line. For an active tectonic region the threshold for this discriminant is $M_L = 3.1$ for earthquakes and $M_L = 3.6$ for explosions for epicentral distances up to 600 km.

ACKNOWLEDGMENTS

We wish to thank Riley Geary for the use of explosion M_L's which he has compiled from the CIT catalog. This research was supported by the Defense Advanced Research Projects Agency (DOD), Nuclear Monitoring Research Office and was monitored by Air Force Geophysics Laboratory under Contract F29601-91-K-DB14. It was also supported by Phillips Laboratory of the Air Force Systems Command under Contract F19628-90-K-0049. Contribution No. 5200, Division of Geological and Planetary Sciences, California Institute of Technology, Pasadena, California.

REFERENCES

Aki, K. (1967). Scaling law of seismic spectrum, *J. Geophys. Res.* **72**, 1217–1231.

Aki, K., M. Bouchon, and P. Reasenberg (1974). Seismic source function for an underground nuclear explosion, *Bull. Seism. Soc. Am.* **64**, 131–148.

Basham, P. W. (1969). Canadian magnitudes of earthquakes and nuclear explosions in southwestern North America, *Geophys. J. R. Astr. Soc.* **17**, 1–13.

Bent, A. L. and D. V. Helmberger (1991). A Re-examination of historic earthquakes in the San Jacinto fault zone, California. *Bull. Seism. Soc. Am.* **81**, 2289–2309.

Brune, J. N. (1970). Tectonic stress and the spectra of seismic shear waves from earthquakes, J. Geophys. Res **75**, 4997–5009.

Cohn, S. N., T. L. Hong, and D. V. Helmberger (1982). The Oroville earthquakes: a study of source characteristics and site effects, *J. Geophys. Res.* **87**, 4585–4594.

Day, S. M. and K. L. McLaughlin (1991). Seismic source representation for Spall, *Bull. Seism. Soc. Am.* **81**, 191–201.

Day, S. M., N. Rimer, and J. T. Cherry (1982). Surface waves from underground explosions with Spall: analysis of elastic and nonlinear source models, *Bull. Seism. Soc. Am.* **73**, 247–264.

Der, Z. A. (1986). Comments on the paper "Estimation of scalar moments from explosion-generated surface waves," by J. L. Stevens, *Bull. Seism. Soc. Am.* **76**, 1822–1824.

Doser, D. I. and R. B. Smith (1989). An assessment of source parameters of earthquakes in the cordillera of the western United States, *Bull. Seism. Soc. Am.* **79**, 1389–1409.

Doser, D. I. (1990). A Re-examination of the 1947 Manix, California, earthquake sequence and comparison to other sequences of the Mojave Block, *Bull. Seism. Soc. Am.* **80**, 267–277.

Dreger, D. S. and D. V. Helmberger (1990). Broadband modeling of local earthquakes, *Bull. Seism. Soc. Am.* **80**, 1162–1179.

Dreger, D. S. and D. V. Helmberger (1991a). Complex faulting deduced from broadband modeling of the February 28, 1990 Upland earthquake ($M_L = 5.2$), *Bull. Seism. Soc. Am.* **81**, 1129–1144.

Dreger, D. S. and D. V. Helmberger (1991b). Source parameters of the Sierra Madre earthquake from regional and local body waves, *Geophys. Res. Lett.* **18**, 2015–2018.

Dreger, D. S. and D. V. Helmberger (1992). Determination of source parameters at regional distances with three-component sparse network data, *J. Geophys. Res.* (in press).

Dziewonksi, A. M., T. A. Chouw, and J. H. Woodhouse (1981). Determination of earthquake source parameters from waveform data for studies of global and regional seismicity, *J. Geophys. Res.* **86**, 2825–2852.

Evernden, J. F., W. J. Best, P. W. Pomeroy, T. V. McEvilly, J. M. Savino, and L. R. Sykes (1971). Discrimination between small-magnitude earthquakes and explosions, *J. Geophys. Res.* **76**, 8042–8055.

Fletcher, J., J. Boatwright, L. Haar, T. Hanks, and A. McGarr (1984). Source parameters for aftershocks of the Oroville, California earthquake, *Bull. Seism. Soc. Am.* **74**, 1101–1123.

Frankel, A. (1984). Source parameters of two $M_L \sim 5$ earthquakes near Anza, California and a comparison with an Imperial Valley aftershock, *Bull. Seism. Soc. Am.* **74**, 1509–1527.

Given, J. W. and G. R. Mellman (1986). Estimating explosion and tectonic release source parameters of underground nuclear explosions from Rayleigh and Love wave observations, *DARPA Report AFGL-TR-86-0171.*

Haskell, N. A. (1967). Analytical approximation for the elastic radiation from a contained underground explosion, *J. Geophys. Res.*, **72**, 2583–2586.

Helmberger, D. V. and D. M. Hadley (1981). Seismic source functions and attenuation from local and teleseismic observations of the NTS Events JORUM and HANDLEY, *Bull. Seism. Soc. Am.* **71**, 51–67.

Herrin, E. and T. Goforth (1977). Phase matched filtering: applications to the study of Rayleigh waves, *Bull. Seism. Soc. Am.* **76**, 1259–1275.

Johnson, L. R. and T. V. McEvilly (1974). Near-field observations and source parameters of Central California earthquakes, *Bull. Seism. Soc. Am.* **64**, 1855–1886.

Johnson, L. R. (1988). Source characteristics of two underground nuclear explosions, *Geophys. J. Int.* **95**, 15–30.

Kafka, A. L. (1990). R_g as a depth discriminant for earthquakes and explosions: a case study in New England, *Bull. Seism. Soc. Am.* **80**, 373–394.

Kanamori, H., J. Mori, E. Hauksson, T. H. Heaton, L. K. Hutton, and L. M. Jones (1992). Determination of earthquake energy release and M_L using TERRAscope, *submitted to Bull. Seism. Soc. Am.*

Kanamori, H. and J. W. Given (1981). Source parameters determined from long period surface waves, *Phys. Earth Planet. Int.* **11**, 312–332.

Lambert, D. G. and S. S. Alexander (1971). Relationship of body and surface wave magnitudes for small earthquakes and explosions, *Final AFTAC Report VELA T/2706, Teledyne Geotech.*

Liebermann, C. R. and P. W. Pomeroy (1969). Relative excitation of surface waves by earthquakes and underground explosions, *J. Geophys. Res.* **74**, 1575–1590.

Ma, K. F. and H. Kanamori (1991). Aftershock sequence of the 3 December 1988 Pasadena Earthquake, *Bull. Seism. Soc. Am.* **81**, 2310–2319.

Marshall, P. D. (1970). Aspects of the spectral differences between earthquakes and underground explosions, *Geophys. J. R. Astr. Soc.* **20**, 397–416.

Mori, J. and A. Frankel (1990). Source parameters for small events associated with the 1986 North Palm Springs, California, earthquake determined using empirical green functions, *Bull. Seism. Soc. Am.* **80**, 278–295.

Müller, R. A. (1973). Seismic moment and long-period radiation of underground nuclear explosions, *Bull. Seism. Soc. Am.* **63**, 847–857.

Müller, R. A. and J. R. Murphy (1971). Seismic characteristics of underground nuclear detonations: Part I. Seismic spectrum scaling, *Bull. Seism. Soc. Am.* **61**, 1675–1692.

Murphy, J. R. and T. J. Bennett (1982). A discrimination analysis of short-period data recorded at Tonto Forest Observatory, *Bull. Seism. Soc. Am.* **72**, 1351–1366.

Patton, H. J. (1988). Source models of the HARZER explosion from regional observations of fundamental-mode and higher mode surface waves, *Bull. Seism. Soc. Am.* **78**, 1133–1157.

Patton, H. J. and G. Zandt (1991). Seismic moment tensors of western U. S. earthquakes and implications for tectonic stress field, *J. Geophys. Res.* **96**, 18,245–18,259.

Peppin, W. A. and T. V. McEvilly (1974). Discrimination among small magnitude events on Nevada test site, *Geophys. J. R. Astr. Soc.* **37**, 227–243.

Richter, C. F. (1935). An instrumental magnitude scale, *Bull. Seism. Soc. Am.* **25**, 1–32.

Richter, C. F. (1958). *Elementary Seismology*, W. H. Freeman, San Francisco.

Romanowicz, B. A. (1982). Moment Tensor inversion of long period. Rayleigh Waves: a new approach, J. Geophys. Res. **87**, 5395–5407.

Saikia, K. C., A. L. Kafka, S. C. Gnewuch, and J. W. McTigue (1990). Shear velocity and intrinsic Q structure of the shallow crust in southwestern New England from R_g wave dispersion, *J. Geophys. Res.* **95**, 8527–8541.

Savino, J. L., L. R. Sykes, R. C. Lieberman, and P. Mollnar (1971). Excitation of seismic surface waves with periods of 15 to 70 seconds for earthquakes and underground explosions, *J. Geophys. Res.* **76**, 8003–8020.

Stevens, J. L. and S. M. Day (1985). The physical basis of m_b:M_s and variable frequency magnitude methods for earthquake/explosion discrimination, *J. Geophys. Res.* **90**, 3009–3020.

Stevens, J. L. (1986a). Estimation of scalar moments from explosion-generated surface waves, *Bull. Seism. Soc. Am.* **76**, 123–151.

Stevens, J. L. (1986b). Reply to Z. Der's "Comments on the paper 'estimation of scalar moments from explosion-generated surface waves'," *Bull. Seism. Soc. Am.* **76**, 1825–1829.

Stump, B. W. and L. R. Johnson (1984). Near-field source characteristics of contained nuclear explosions in tuff, *Bull. Seism. Soc. Am.* **74**, 1–26.

Stump, B. W. (1985). Constraints on explosive sources with Spall from near-source waveforms, *Bull. Seism. Soc. Am.* **75**, 1312–1325.

Taylor, S. R. and G. E. Randall (1989). The effects of Spall on regional seismograms, *Geophys. Res. Lett.* **16**, 211–221.

Thio, H. K. and H. Kanamori (1991). A surface wave study on the structure of the crust and upper mantle under Southern California (*abstract*) *Eos Trans AGU*, **72**, no. 44, 324.

Thio, H. K. and H. Kanamori (1992). Moment tensor inversions in Southern California using surface waves recorded by TERRAscope (*abstract*) *Eos Trans AGU*, **73**, no. 43, 376.

Viecelli, J. A. (1973). Spallation and the generation of surface waves by an underground nuclear explosion, *J. Geophys. Res.* **78**, 2475–2487.

Vidal, A. and L. Munguia (1991). Local magnitude and source parameters for earthquakes in the Peninsular Ranges of Baja California, Mexico, *Bull. Seism. Soc. Am.* **81**, 2254–2267.

Woods, B. B., C. K. Saikia and D. V. Helmberger (1992). An energy discriminant for regional seismic events, *Eos Trans AGU*, **73**, no. 43, 359.

Woods, B. B. and Harkrider, D. G. (1993). Determining surface wave magnitudes from regional NTS data, *Geophys. J. Int.* (submitted).

Wyss, M. and J. N. Brune (1968). Seismic moment, stress, and source dimensions for earthquakes in the California-Nevada region, *J. Geophys. Res.* **73**, 4681–4694.

Zhao, L. S. and D. V. Helmberger (1993). Source estimation from broadband regional seismograms, *Bull. Seism. Soc. Am.* (submitted).

Zhao, L. S. and D. V. Helmberger (1991). Broadband modelling along a regional shield path, Harvard recording of the Saguenay earthquake, *Geophys. J. Int.* **105**, 301–312.

SEISMOLOGICAL LABORATORY 252-21,
CALIFORNIA INSTITUTE OF TECHNOLOGY
(B.B.W., S.K., D.V.H.)

Manuscript received 18 August 1992